Assessment of the performance and radiation damage effects under cryogenic temperatures of a P-channel CCD204s

Conference or Workshop Item

Assessment of the performance and radiation damage effects under cryogenic temperatures of a P-channel CCD204s

Neil J. Murray, Andrew D. Holland, Jason P. D. Gow, David J. Hall, Konstantin D. Stefanov, et al.

Neil J. Murray, Andrew D. Holland, Jason P. D. Gow, David J. Hall, Konstantin D. Stefanov, Ben J Dryer, Simeon Barber, David J. Burt, "Assessment of the performance and radiation damage effects under cryogenic temperatures of a P-channel CCD204s," Proc. SPIE 9154, High Energy, Optical, and Infrared Detectors for Astronomy VI, 91540P (23 July 2014); doi: 10.1117/12.2069289

Event: SPIE Astronomical Telescopes + Instrumentation, 2014, Montréal, Quebec, Canada

Assessment of the Performance and Radiation Damage Effects under Cryogenic Temperatures of P-channel CCD204s

Neil J. Murray[1], Andrew D. Holland[1], Jason P. D. Gow[1], David J. Hall[1], Konstantin D. Stefanov[1], Ben J. Dryer[1], Simeon Barber & David J. Burt[2]
[1]Centre for Electronic Imaging, Open University, Milton Keynes, MK7 6AA, UK
[2]e2v technologies plc., 106 Waterhouse Lane, Chelmsford, CM1 2QU, UK

ABSTRACT

CCDs continue to be the detector of choice for high resolution and high performance space applications. One perceived drawback is their susceptibility to radiation damage, in particular the formation of trap sites leading to a decrease in charge transfer efficiency. To that end, ESA has started a programme to investigate a new generation of devices based upon p-channel technology. The expectation is that once mature, p-channel devices may offer a significant increase in tolerance to proton radiation over traditional n-type buried channel CCDs. Early studies of e2v devices to assess the radiation hardness of p-channel devices were limited by the quality of devices available, however more recently, good quality p-channel CCD204s have been manufactured and studied.

A more detailed evaluation of p-channel CCDs is now underway to realise the full potential of the technology for use in future high radiation environment space missions.

A key aspect is the development of a cryogenic test rig that will allow for the first time a direct comparison of the radiation damage effects when the irradiation is performed both traditionally unbiased at room temperature and cryogenically with the device operational. Subsequent characterisations will also be performed on the cryogenic device after periods of storage at room temperature to investigate the potential annealing effects upon the lattice damage.

Here we describe and present early results from an extensive programme of testing which will address all key performance parameters for p-channel CCDs, such as full electro-optical characterisation, assessment of radiation hardness and investigation of trap species.

Keywords: CCD, p-channel, cryogenic irradiation, proton irradiation, CTI, CTE, trap pumping, annealing

1. INTRODUCTION

It has long been believed that CCDs fabricated with a p-type buried channel on an n-type substrate would offer a significant increase in tolerance to proton radiation over traditional n-type buried channel on p-type substrates. This is due to the substitution of the highly affected phosphorus dopant atoms (generating E-centre traps that have an emission time comparable to the frame period) in the charge transfer channel under proton irradiation with the less affected boron dopant atoms. Early studies of e2v devices to assess the radiation hardness of p-channel devices were limited by the quality of devices available, however more recently, good quality p-channel CCD204s have been manufactured and studied. This has highlighted the fact that the traditional understanding of intrinsic trap species present in CCDs and the generation of additional trap sites through radiation damage is based on ~40 years of research performed on n-channel devices and there is little on p-channel devices manufactured by e2v technologies plc. Therefore a more detailed evaluation of p-channel CCDs is required to realise the full potential of the technology for use in future space missions subject to high radiation environments.

*n.j.murray@open.ac.uk; tel: +44 (0)1908 332769; fax: +44 (0)1908 655910; http://www.open.ac.uk./cei

High Energy, Optical, and Infrared Detectors for Astronomy VI, edited by Andrew D. Holland, James Beletic, Proc. of SPIE Vol. 9154, 91540P · © 2014 SPIE · CCC code: 0277-786X/14/$18 · doi: 10.1117/12.2069289

This paper describes an extensive programme of testing with initial results, which will address all key performance parameters for p-channel CCDs, such as full electro-optical characterisation, assessment of radiation hardness and investigation of trap species. A key aspect is the development of a cryogenic test rig that will allow for the first time a direct comparison of the radiation damage effects when the irradiation is performed both traditionally unbiased at room temperature and cryogenically with the device operational. Subsequent characterisations will also be performed on the cryogenic device after periods of storage at room temperature to investigate the potential annealing effects of the lattice damage.

Previous work with p-channel CCDs indicated an improvement in radiation hardness when compared with n-channel CCDs[1,2,3]. However, the method of the comparison was called into question due to differing measurement techniques, operating temperatures, clocking and device structure[4]. To resolve this uncertainty, a comparative study between n- and p-channel to benchmark the same devices in terms of radiation hardness is required. This study will evaluate the intrinsic performances and degradation under proton irradiation of the p-channel CCD204, to allow direct comparison with the existing characterised n-channel version.

2. EARLY e2v P-CHANNEL CCD HISTORY

e2v have found it relatively straight-forward to fabricate p-channel devices by a simple reversal of the dopant types with the electrodes remaining n-type doped. The operating voltages are the same as n-channel but with a reversal of polarity and photo-generated holes are collected rather than electrons.

First generation devices were based around the early CCD02 format with 385×578 22 µm square pixels, shown far left in Figure 1. Thin gate technology and inverted mode implants were included with the intention that the device would be 'hard' with respect to both ionising and proton irradiation, *i.e.* low flat-band voltage shift from thin-gate, low dark current from inverted mode and minimal loss of CTE through displacement damage. However, at the time it was not realised that the electrons used for pinning have a considerably increased ionisation coefficient (compared with the holes used for n-channel) and, with the thin gate dielectric, this resulted in much higher levels of clock-induced charge[5]. It was therefore found to be very difficult to find a useful operating point. Another consequence of the differing ionisation coefficients, and hence conclusion of this work, was that it would be impractical to produce gain registers for signal multiplication in p-channel devices.

The second generation of devices were manufactured on high resistivity bulk silicon (Hi-rho), with the intention of being fully depleted by large gate-to-substrate bias when back thinned to >100 µm. A front-illuminated CCD227-80 is shown centre-left in Figure 1. Initial characterisations of the front-illuminated CCD227 were performed and it was found that, although the general pixel response non-uniformity was similar to that of the n-channel devices, there was a significant increase in bright pixel defects and hence it was concluded that the cosmetic performance of p-channel was worse than n-channel due to the lower quality of the silicon used[6,7]. Initial measurements also suggested that p-channel devices exhibited higher dark current generation rates than in n-channel samples and that devices would require cooling to approximately 20 degrees lower to achieve the same dark signal level as n-channel.

A third generation of CCD47-20 devices were fabricated on n-type epitaxial layer silicon on n+ substrate and characterised by the CEI in 2008 in terms of CTE, both pre- and post-irradiation with protons. Although it was found that the initial CTE was very poor, the p-channel device offered better performance at levels of irradiation greater than ~2E9 p.cm-2 (10 MeV equivalent)[8]. The dark signal at room temperature was found to be twice that of n-channel CCDs; however the increase with proton fluence was comparable to n-channel. From this study it was concluded that the poor performance in respect of CTE was a consequence of using epitaxial material, leading to a far higher concentration of intrinsic trap species. In the case of p/p+ material used for traditional n-channel devices, if the substrate has a relatively high oxygen content, which is usually the case with Czochralski (CZ) material, precipitates naturally form which attract

contamination and crystallographic imperfections away from the epi-layer and into the neutral substrate. The mechanism is termed "intrinsic gettering" and the quality of the layer improves with the high temperature processing steps. This mechanism does not happen with the n/n+ material used to manufacture p-channel devices and in fact the quality worsens with high temperature processing, hence the inferior results.

From these findings the conclusion is that p-channel devices have to be fabricated on bulk non-epitaxial material. The fact that there is no natural etch-stop at the n/n+ interface means that only relatively thick deeply-depleted devices are likely to be fabricated, where very precise thickness control is not necessary.

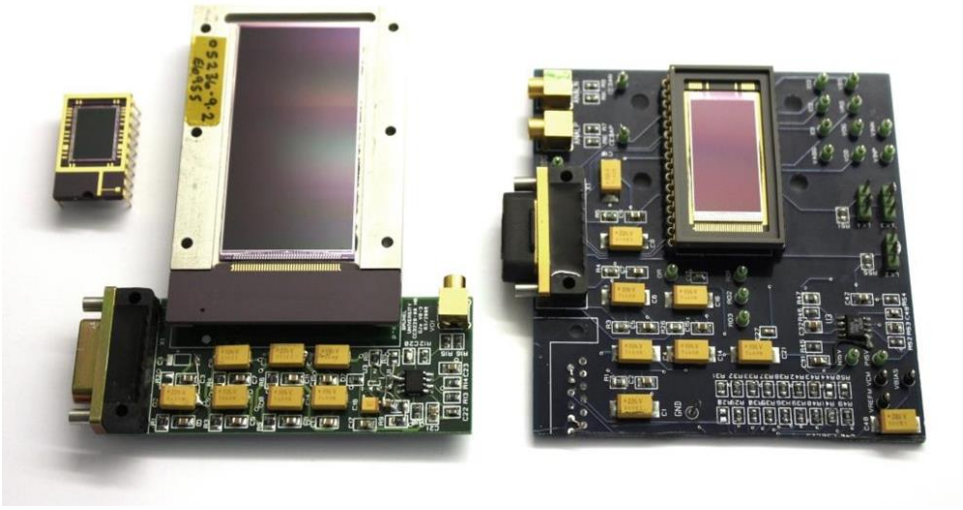

Figure 1. Early generations of e2v full-frame p-channel CCDs (left: CCD02, centre: CCD227-80, right: CCD47-20)

3. P-CHANNEL CCD204-22

In 2010, e2v manufactured two batches of back-illuminated p-channel CCD204-22 for ESA, shown in Figure 2 (left), from high resistivity bulk n-type silicon and thinned to ~70 µm. This thickness was 'chosen' to ensure good X-ray QE for ^{55}Fe, whilst keeping lateral diffusion effects to a minimum simplifying the measurement of CTE. Devices were of full-frame architecture with 4k×1k×12 µm square pixels, shown Figure 2 (right). Similar to the n-channel CCD204 devices, a parallel hole-injection structure was included to artificially inject charge for calibration and trap filling purposes. Aside from the reduced imaging area and charge injection structure, the architecture of the device is near-identical to the e2v n-channel CCD203-82[9].

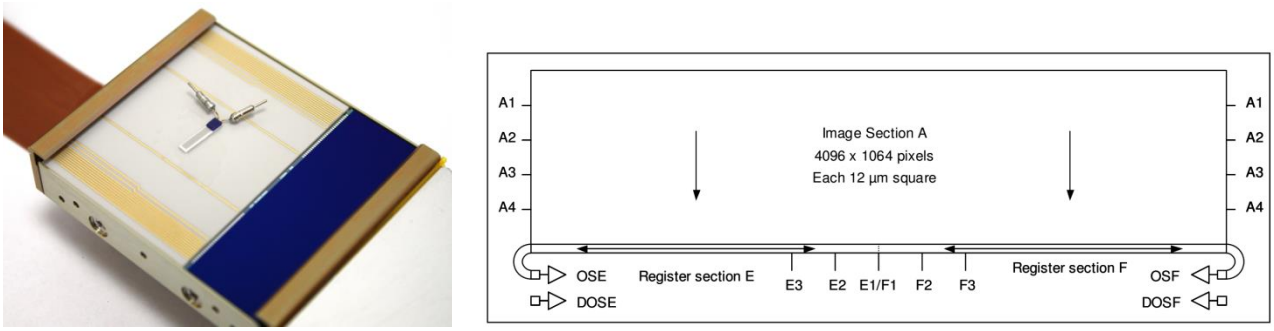

Figure 2. Left: P-channel CCD204-22 in CCD203 metal package with additional temperature sensor glued to ceramic spacer. Right: CCD204 architecture (e2v technologies)

The aim of the ESA activity was to provide for the first time a direct comparison of n- and p-channel performance on devices with the same architecture, operating conditions and measurement methods. However this would ultimately prove to limit the performance of the p-channel devices, despite the very good quality of the devices[10].

Six devices were delivered to the CEI for characterisation, including CTE measurements both before and after irradiation with protons. The combination of operating temperature (153K) and clock timings specified for use in the study meant a particular trap species had a release time constant similar to the line transfer period and hence lead to a significant reduction in CTE and limiting the reported performance. Some initial optimisation was performed, beyond the scope of the previous study and prior to the devices being returned to ESA. This began by using the trap-pumping technique to investigate the suppression of charge transfer traps in the parallel array by reducing the parallel transfer rate[11]. Parallel CTE was then derived from the gradient of X-ray stack plots, whilst exploring the line transfer rate. The effect on parallel CTE is shown in figures 3 and 4.

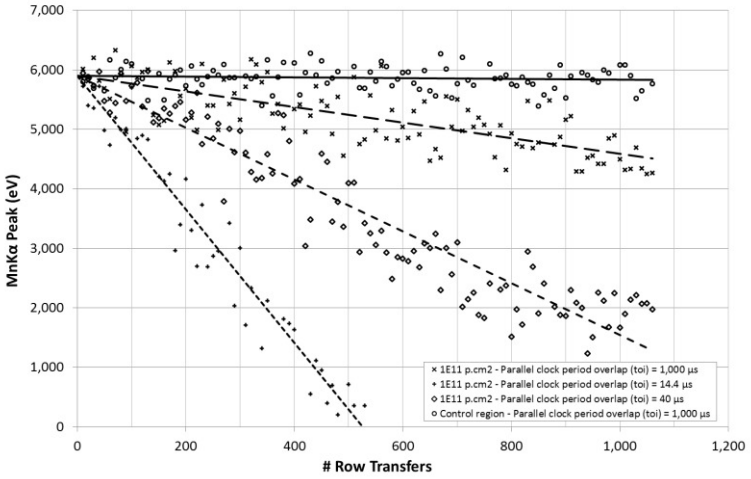

Figure 3. X-ray stack plots of 5,898 eV events in irradiated section of a p-channel CCD204 as a function of parallel transfer time. Irradiated section was 1E11 p.cm^{-2} (10 MeV equivalent) and T=153K.

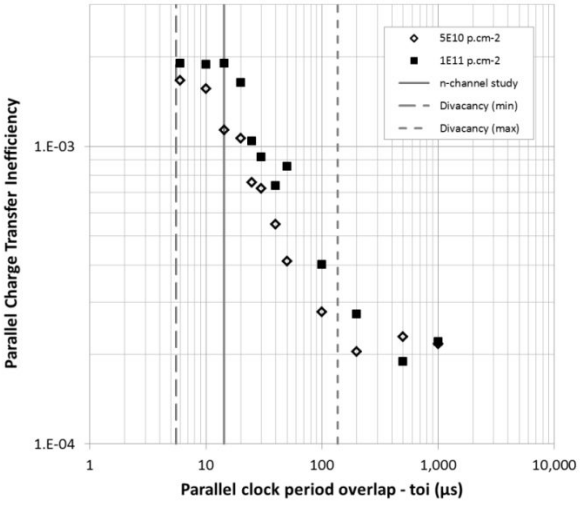

Figure 4. P-channel CCD204 parallel CTI vs. parallel clock period

It can be seen in Figure 3 that by using the parallel clock period used in the earlier n-channel study (toi = 14.4 µs)[12], charge is completely deferred from the original charge packet before it traverses the 1,064 element array through the highly irradiated section and hence no peak energy can be resolved. Hence the fit reaches 0 eV in the y-axis before the number of transfers has reached 1,064 parallel transfers (the physical size of the CCD204-22 imaging array). Figures 4 and 5 show the improvement in CTE observed by 5,898 eV events simply by increasing the parallel clock period overlap. Note that the previous study was constrained to parallel clock periods of 14.4 µs that offered the worst performance in terms of parallel CTE.

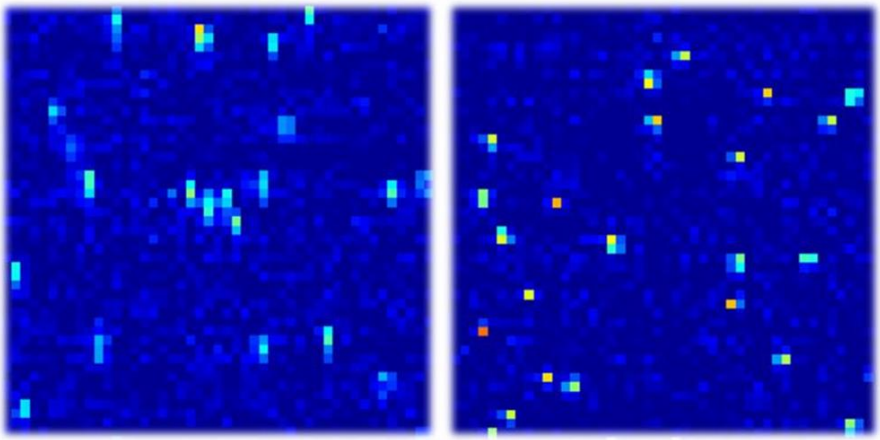

Figure 5. Example 5,898 eV events after ~1,000 parallel transfers through p-channel CCD204 proton irradiated to 1E11 p.cm-2 (10 MeV equivalent) at 153K. Left: Traditional n-channel line transfer timings (14.4 µs parallel clock overlaps) showing poor parallel CTE. Right: Transfer time increased by ~100 times showing good parallel CTE

With a greater understanding of p-channel performance in terms of CTE, some of the discrepancies reported earlier[4] can now be understood. The aim of this current study is to use this knowledge to realise the very best performance that can be achieved with p-channel CCD204 devices. To this end, a detailed investigation into the device physics and optimisation of the detectors is currently being performed, prior to a full proton radiation study, including the comparison with cold irradiation and potential annealing effects during room temperature storage. A significant modelling activity is also underway in parallel that will allow recommendations to be made as to the design of future devices and their operating conditions for optimal performance. Within the scope of this activity it is not possible to develop a full end-to-end p-channel CCD model and so the model concentrates on that which is required to gain an understanding of the experimental results, charge storage, trap parameters/densities and device performance.

4. ELECTRO-OPTICAL CHARACTERISATIONS

A complete Electro-Optical (EO) characterisation of seven p-channel CCD204 devices is being performed that includes: optimal operational temperature, charge to voltage conversion factor, global and local photo-response non-uniformity, read out noise, non-linearity, image and register full well capacity, dark signal, dark signal non-uniformity, defects in darkness, charge injection uniformity, parallel and serial charge transfer efficiency, point spread function, modulation transfer function, quantum efficiency and trap identification by pumping. This will not only gain a thorough understanding of the device behaviour and comparison with the previous study, but to provide inputs to the parallel modelling and simulation activity. Devices were optimised in terms of biasing levels, clocking schemes and frequencies using a proton irradiated device from the previous study.

To expedite the study, testing is being performed in parallel using both Dark and Light Test cameras, shown in Figure 6. Data acquisition and analysis software is scripted in MATLAB to automate as much of the process as possible.

The Dark test camera is shown in Figure 6 (left) employs an Oxford Instruments XTF5011/75-TH X-ray tube, with a tungsten anode that will be used to fluoresce a manganese target held at 45° to the incident X-ray beam to provide 5,898 eV photons for calibration and charge transfer efficiency (CTE) measurements. In addition 500 nm LEDs are included within the chamber to provide a roughly uniform illumination for optical background injection used in the trap-pumping, Photon Transfer Curve (PTC) and CTE measurements.

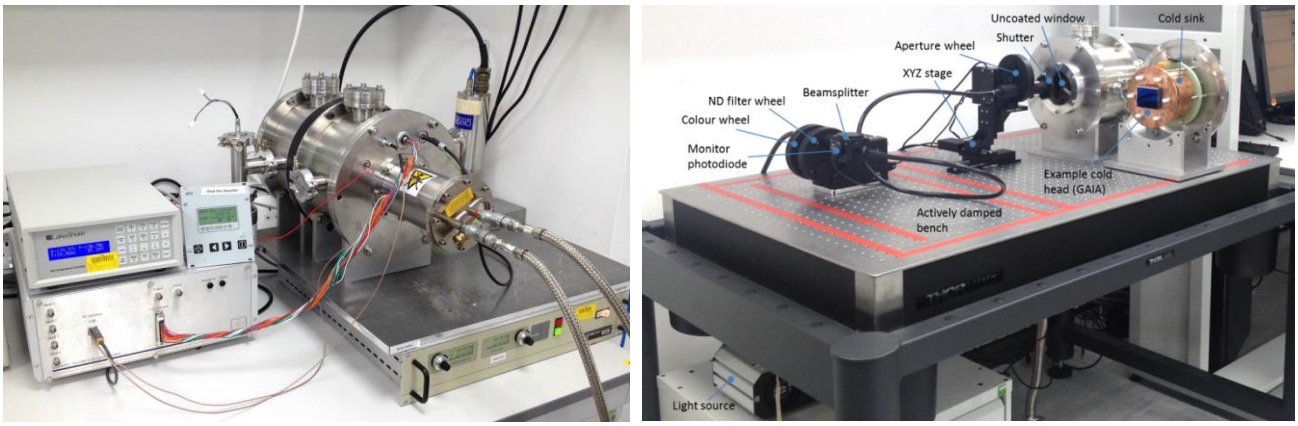

Figure 6. Left: Dark test camera. Right: Light test camera (dark boxes removed)

The Light test camera has been designed to be computer controlled such that all tests can be scripted to run without user input. A broadband halogen light source is coupled via a liquid guide to a shutter and pair of filter wheels that select the wavelength (380, 450, 500, 700, 900 and 950 nm, all with 10 nm FWHM) and intensity (0.01, 0.1, 1, 10, 50 and 100% transmission). A beam splitter redirects the light into both a dedicated photodiode (Thorlabs S120VC) for monitoring stability and into the XYZ controlled projection optics. The XYZ translation stages have a range of 50 mm in each direction and a step size of 50 nm. A third filter wheel selects the pattern of the desired projection (5 µm spot, 20 µm spot, 5 µm horizontal slit, 5 µm vertical slit, USAF test chart and engineered diffuser) and this is de-magnified through the glass entrance window to the vacuum chamber using a matched achromatic doublet pair (9.1 µm r.m.s.).

The optical system sits on top of an actively stabilised optical bench and is covered within two separate dark boxes, shown in Figure 7 (left); one box to cover the light conditioning and one box to cover the projection system. A further dark box covers both of these, shown in Figure 7 (right).

Figure 7. Light test camera dark boxes. Left: internal boxes (lids removed). Right: Cover

The cold bench that supports the detector within the Light test camera is connected to a large thermal mass, as shown in Figure 8, so that the CryoTiger refrigeration pump can be disabled during some tests to minimise vibration in the system.

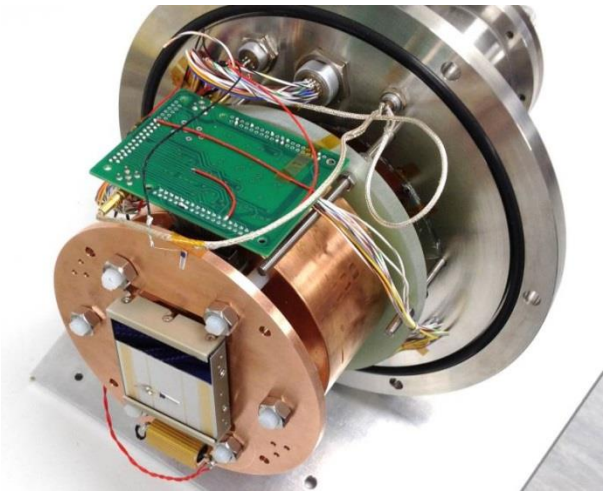

Figure 8. Light test camera head with p-channel CCD204

During testing, CCDs will be clamped onto a copper cold bench connected to a CryoTiger® refrigeration system. Thermal stabilisation to ± 0.2 K is provided using a Lakeshore controller and resistive heater in thermal contact with the copper cold bench that can be mechanically configured to the following temperature ranges: 143 K to 193 K, 193 K to 243 K and 243 K to 293 K. Device temperature is measured from a platinum resistance thermometer (PT1000) glued to the ceramic spacer adjacent to the silicon die, shown in Figure 8.

5. DEVICE OPTIMISATION

Each set of device parameters are optimised in one day using the Dark Test Camera, using analysis of charge injection (clock and bias levels), trap-pumping (clock frequency/pattern) and CTE measurement (temperature).

The optimum clock amplitude high is equal to the channel parameter (buried channel potential). Optimal values for remaining biases can be calculated from this value. To find the channel parameter the Injection Drain (ID) potential of the charge injection structure is increased from -24 V until the point that charge is injected continuously into the array (approx. -10 V). The level is reduced again in small steps (~0.1 V) until the injection stops. The value of ID is now approximate to the buried channel potential and this is used to calculate appropriate clock and bias values to be baselined for subsequent testing of that particular device.

The trap or pocket-pumping technique can be used to highlight the locations, efficiencies and properties (*e.g.* emission time constants and capture dynamics) of traps present in the charge transport channel of a CCD[11,13]. Parameters such as the transfer rate in the process can be explored to minimise the 'pumping' efficiency, leading to improved charge transfer efficiency (CTE) during normal readout[11]. Trap-pumping is performed on top of a background of approximately 1,600 holes in the image area. The optimal line transfer rate is found by measuring the density of pixels in the image area that have signal >3σ above the background after 3,000 cycles of trap-pumping in the parallel direction with a 10 ms pause between. The densities of traps are plotted against different parallel clock periods (toi) and the minimum chosen to define the optimum line transfer time. Based on the optimisation performed after the previous study and discussed in Section 3, the following parallel clock overlap periods are used: 10 µs, 30 µs, 50 µs, 100 µs, 200 µs, 300 µs, 500 µs and 1,000 µs.

The densities of traps highlighted in the image area by trap-pumping are in line with expectations following the brief optimisation of the p-channel CCD204 after the previous study. The example parallel trap pumped images shown in Figures 9 and 10 are acquired with a device proton irradiated under the previous study to 4E9 p.cm-2 and 2E9 p.cm-2 (10 MeV equivalent) and cooled to 153K. As the parallel clock period is increased, charge is more likely to be released into its original charge packet and hence the 'pumping' efficiency and measured trap density is reduced. Trap densities from different regions in this device are shown in Figure 11. Datasheet and coincident clocking schemes are explored, where charge is confined under image electrode sequences of 2-3-2-3-2-3-2-3-2 and 2-2-2-2-2 respectivly[11]. From these data, a parallel clock period of 500 µs was chosen for optimal line transfer using the datasheet clock pattern in all further measurements at 153K.

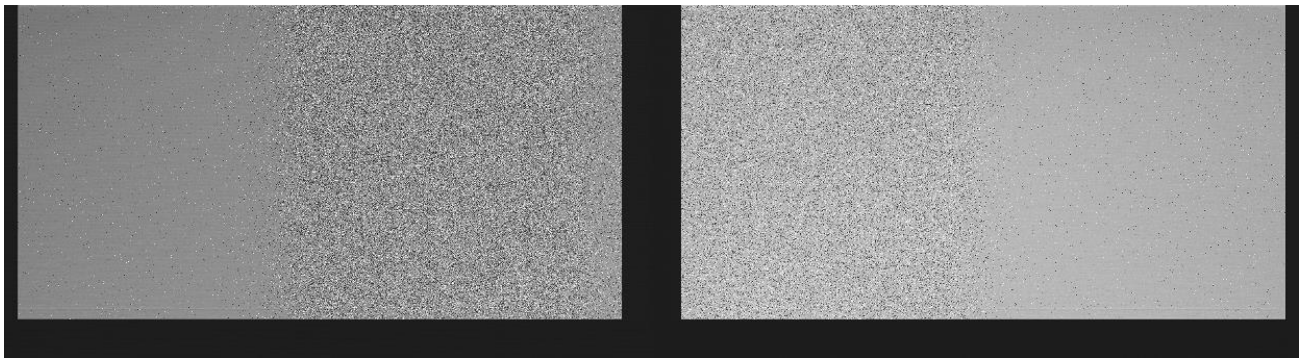

Figure 9 – Trap pumped image example with 10 µs parallel clock period from p-channel CCD204-22 (#10092-02-03), proton irradiated in image regions to cente-left and centre-right of 4E9 p.cm-2 and 2E9 p.cm-2 respectively. Image is composed of two-channel readout. Serial prescans are obseved to the left and right most columns (black) in the image. Serial overscan is in the centre. Two hundred rows of parallel overscan (also black) are observed at the bottom

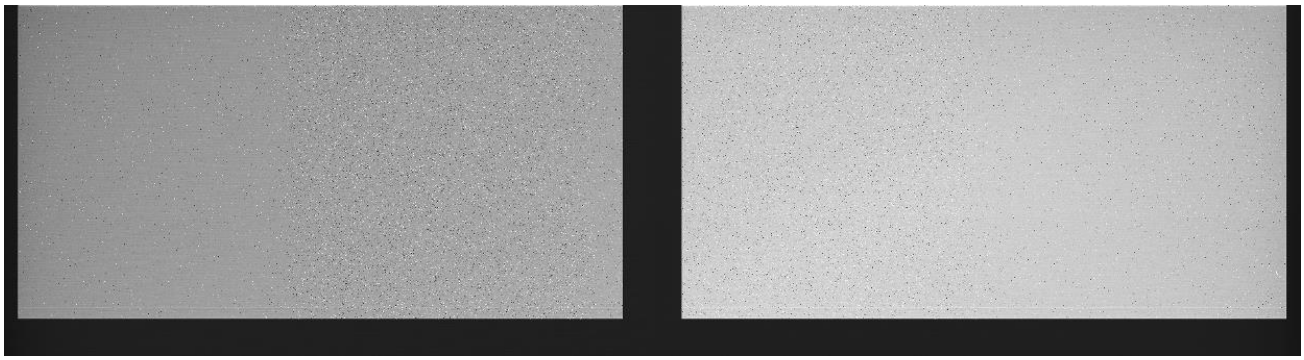

Figure 10 – Trap pumped image example with 1,000 µs parallel clock period from p-channel CCD204-22 (#10092-02-03), proton irradiated in image regions to cente-left and centre-right of 4E9 p.cm-2 and 2E9 p.cm-2 respectively. Image is composed of two-channel readout. Serial prescans are obseved to the left and right most columns (black) in the image. Serial overscan is in the centre. Two hundred rows of parallel overscan (also black) are observed at the bottom

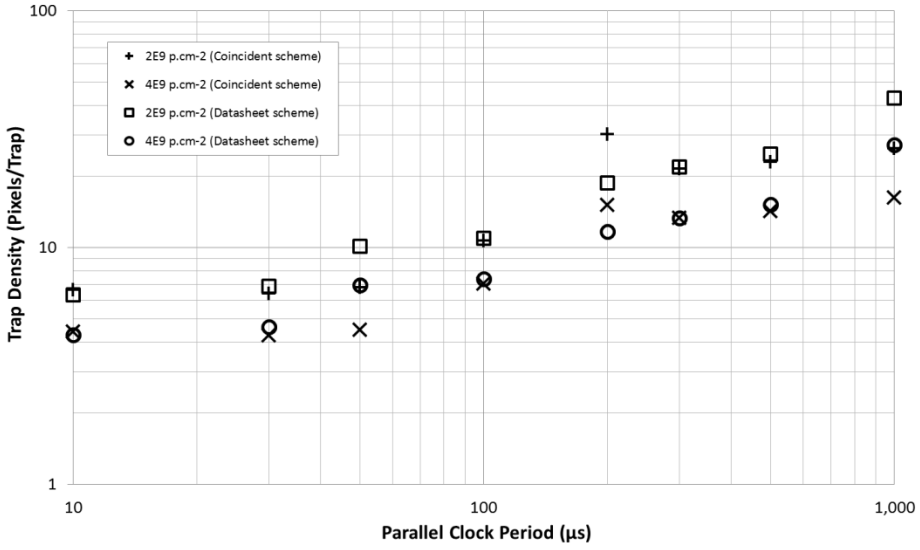

Figure 11. Density of traps in image area as a function of parallel clock period and pattern

Similarly, the optimal pixel rate was found by measuring the density of register elements that have signal >3σ above the background after 3,000 cycles of trap-pumping with 1/3 the pixel period (T_{rr}) pause between. Figure 12 shows an example image used to perform the measurement, whereby the image array is illuminated with 1,600 holes and then after each parallel transfer into the register trap-pumping is performed prior to the line readout. The densities of traps are plotted against different pixel periods in Figure 13 and used to define the optimum pixel rate. Initially the following pixel rates will be used although these may be subject to change: 50 kHz, 70 kHz, 100 kHz, 150 kHz, 200 kHz, 250 kHz and 500 kHz.

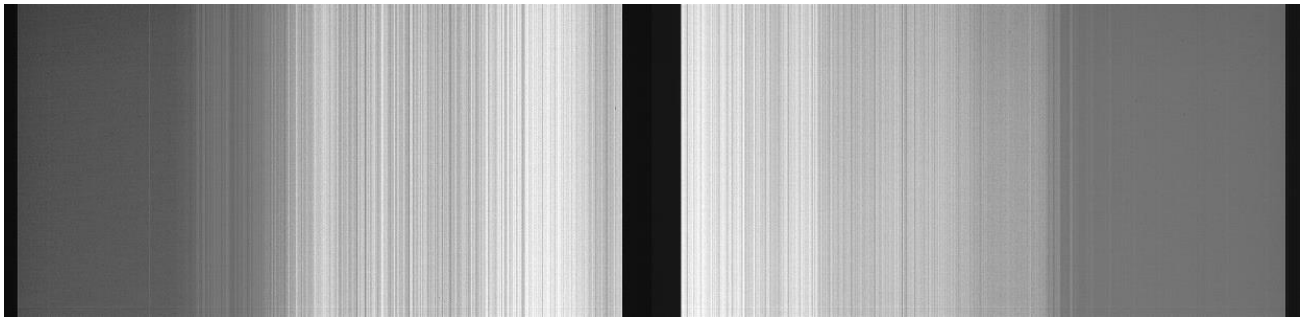

Figure 12. Trap pumped example from p-channel CCD204-22 (#10092-02-03), proton irradiated in register regions to cente-left and centre-right of 4E9 p.cm-2 and 2E9 p.cm-2 respectively. 200 kHz equal mode serial clock frequency

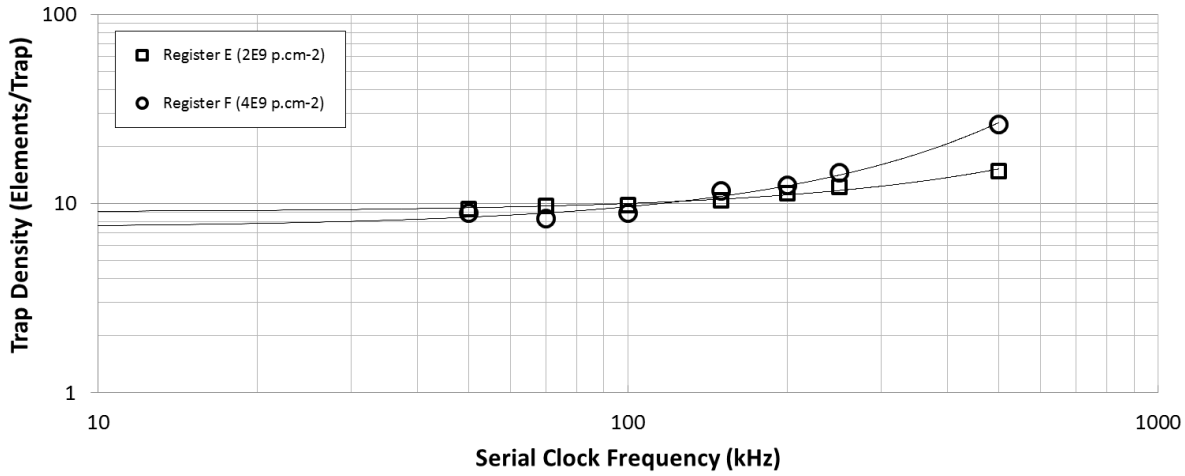

Figure 13. Density of traps in the register area as a function of serial clock frequency

From these data a pixel frequency of 200 kHz would be chosen. However, it must be noted that the trap pumping technique only highlights traps with an emission time constant similar to the transfer time. At the operating temperature of 153K, the emission time is significantly longer than the serial clock periods at 200 kHz and although the pumping efficiency is low, the first pixel response would indicate a CTE problem. Therefore a slower register speed is appropriate and 50 kHz was chosen for subsequent testing.

Temperature optimisation is performed using the Extended Pixel Edge Response (EPER) method to measure the parallel and serial CTI at a signal size of ~160k holes. These are both plotted as a function of temperature in 5 K steps in the range 143 K to 203 K. The optimum temperature is defined as where the best parallel and serial CTI coexist. Figure 14 shows both parallel and serial temperature datasets and shows the optimum temperature to be approximately 183K,

although this is the general case for all-round good performance. The temperature curves in Figure 14 are overlaid on theoretical p-channel trap data[14] and shown in Figure 15. Here we see strong correlation with increased CTI for temperature and clocking periods that are close to the divacancy and the increase when timings move 'closer' to the carbon interstitial.

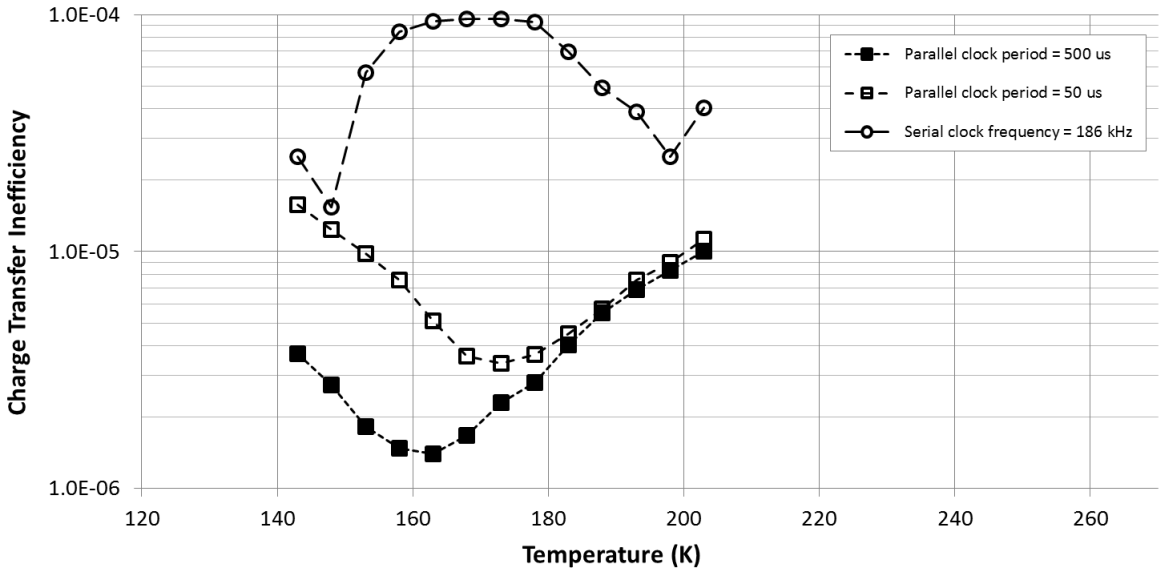

Figure 14. Parallel and serial CTI measurements as a function of operating temperature

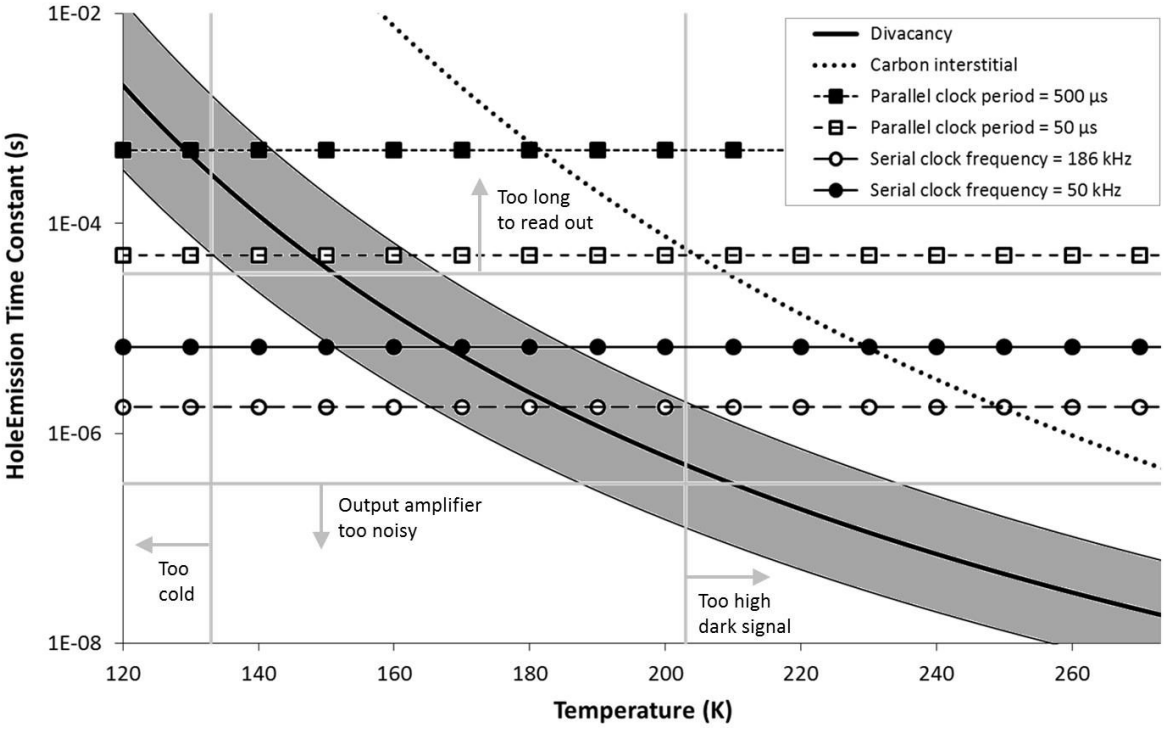

Figure 15. Theoretical p-channel trap emission times with suggested practicable operating parameters window for CCDs

6. INITIAL RESULTS

6.1 Charge to voltage factor

The Charge to Voltage conversion Factor (CVF), or amplifier responsivity is the ratio of output voltage that can be sampled by the CCD for a given charge packet of holes. The CVF can be measured by analysing Mn-Kα X-ray events (5,898 eV) in an image and with knowledge of the gain of the camera electronics. The CVF measured for output nodes E and F of a sample p-channel CCD204 were 4.6 $\mu V/h^+$ and 1.4 for output circuit modes 1 and 2 respectively and are comparable to the n-channel CCD204.

6.2 Global and local photo response non-uniformity

For a uniform illumination there will be a difference in signal sampled by one pixel to another due to variations in pixel geometry. This difference is termed the Photo Response Non-Uniformity (PRNU). The Global PRNU represents the standard deviation of all pixels expressed as a percentage of the median value. The local PRNU represents the standard deviation of all pixels expressed as a percentage of the average signal from the mean value from a window of surrounding pixels and typically measures lower, taking into account any edge-roll off effects that may be observed in thicker devices and non-uniformity of the flat-field exposure. PRNUs are measured at three wavelengths (500, 700 and 900 nm) at a signal level of approximately ¼ full well, so that any charge redistribution effects during collection remain negligible. The PRNUs measured for image sections AE and AF of a sample p-channel CCD204 are shown in Table 1.

Wavelength (nm)	Section AE Global PRNU (%)	Section AE Local PRNU (%)	Section AF Global PRNU (%)	Section AF Local PRNU (%)
500	1.22	0.53	1.78	0.55
700	1.36	0.54	2.26	0.57
900	1.12	0.49	2.28	0.51

Table 1. Global and local photo response non-uniformity measurements

6.3 Readout noise vs. pixel frequency

The readout noise is calculated by first measuring the standard deviation of pixels containing zero signal in ADU (pixels from serial overscan) and then subtracting from this value, in quadrature, the noise contribution arising from the sampling electronics. The system gain calibration is found by the detector's response to Mn-Kα photons (5,898 eV) and is used to convert the readout noise into holes RMS. The data are plotted in Figure 16 in terms of the sampling bandwidth of the CDS processor for comparison to e2v's n-channel CCD204 model and show good agreement.

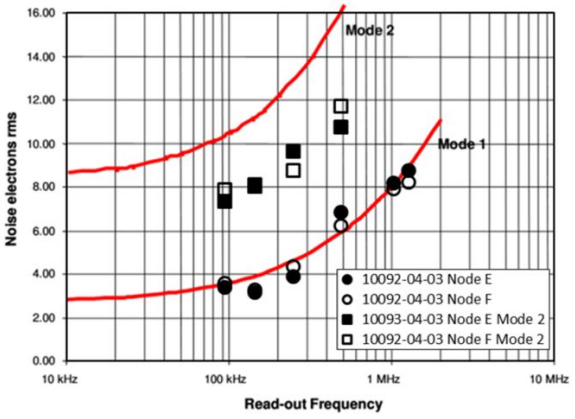

Figure 16. Readout noise vs. sampling bandwidth and comparison to e2v n-channel models. Note that the Mode 2 data shown here are recorded with V_{OG2} = 10V rather than 20 V and so the responsivity is higher, resulting in a lower noise than the model

6.4 Dark signal

Dark signal is charge generated within the image area in the absence of light and is reported in holes/pixel/minute for a given operating temperature. Values of dark signal are measured over temperatures between 143 K and 233 K and are shown in Figure 17 for a sample device.

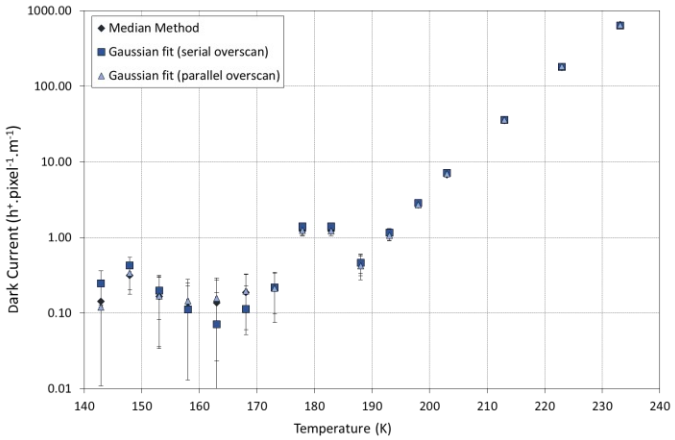

Figure 17. Dark signal vs. temperature

6.5 Defects in darkness

A bright defect is classified as a pixel that, in the absence of light, generates signal in excess of 300 holes/pixel/minute at 173 K. For a sample device of 4.3 Mpix, zero bright defects were measured.

6.6 Parallel charge transfer efficiency

The parallel Charge Transfer Efficiency (CTE) is defined as the average fraction of signal moved in one row transfer. Parallel CTE is measured from X-ray signal loss (5,898 eV input), Extended Pixel Edge Response (EPER) and First Pixel Response (FPR) for comparison. For EPER and FPR measurements, the same image data are used with bias charge levels of: 1.6k, 4k, 10k and 20k holes. In all cases, the CTE is measured with and without an optical background of ~100 holes injected prior to read out. Parallel CTE measurements are shown in Figure 18 of an unirradiated CCD204.

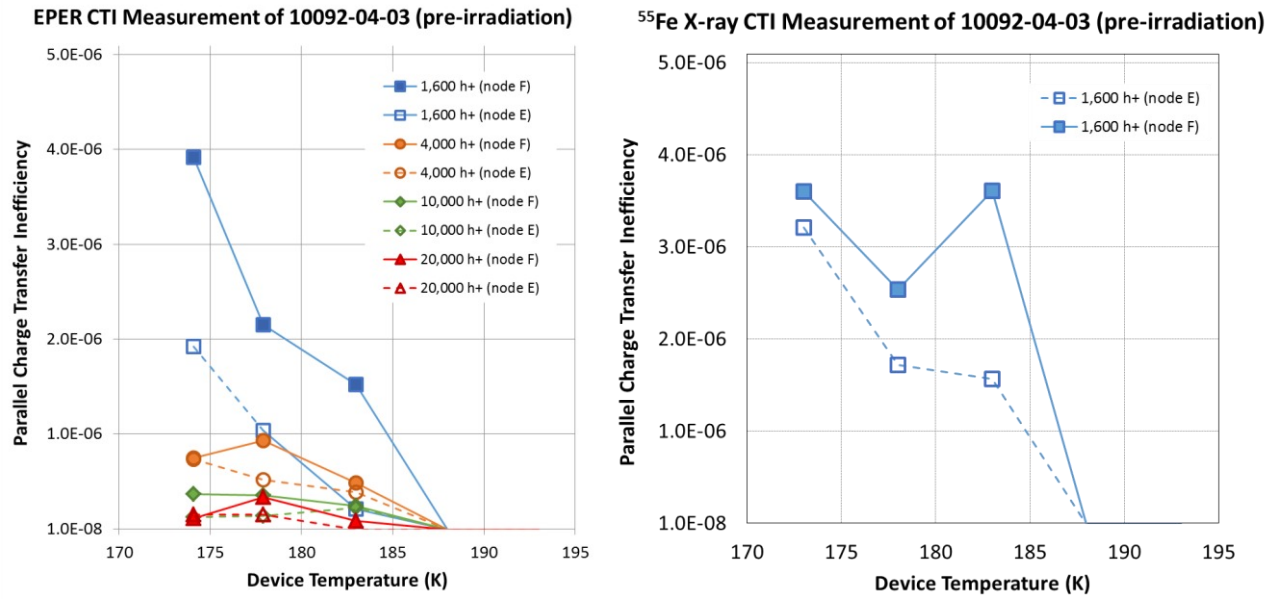

Figure 18. Parallel CTE measurements. Left: Measured from EPER. Right: Measured from ^{55}Fe peak shift

7. PROTON RADIATION TEST CAMPAIGN

Three devices will be irradiated using protons; two devices will be irradiated at room temperature and the third cryogenically. A fourth device will be taken to the irradiation facility, but not irradiated and held as a control to assess any non-radiation induced systematic drift of the test facilities during the full electro-optical testing of each device following the irradiation campaign. The facility selected to perform the irradiation is the Synergy Health Ion Beam based in Harwell, UK and can provide protons between 0.5 MeV and 7.5 MeV. The proton irradiation will be performed under vacuum using 7.4 MeV protons and a summary of the levels to be delivered to the devices is given in Table 2. The facility was selected because it can provide lower energy protons than used during the previous study, limiting the impact of neutron damage to the CCDs. Harwell is also conveniently located which reduces the risk associated in transporting the CCDs, vacuum chamber and camera system required to perform a cryogenic irradiation.

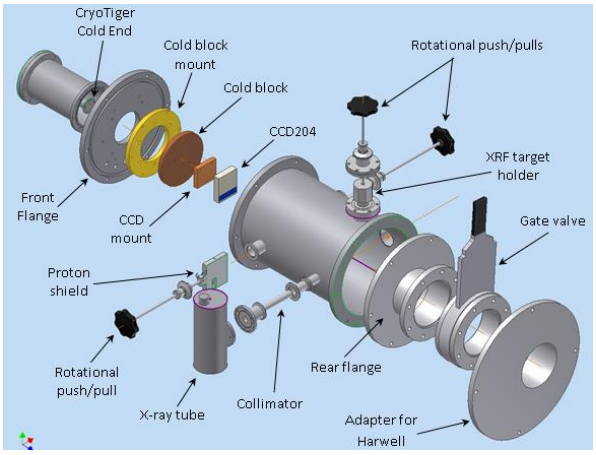

Figure 19. Exploded schematic of the cryogenic chamber[15]

An exploded schematic of the CCD irradiation chamber is illustrated in Figure 19. The push pull on the top of the chamber allows the XRF target to be moved out of the proton beam during the irradiation, it can then be lowered to allow post irradiation CTI measurements to be made. The push-pulls at the side of the chamber will allow two different radiation shields to be moved in front of the CCD, without the need to bring the chamber back to room pressure ensuring efficient operation and allowing for the option to provide two fluence levels to the cryogenically irradiated CCD. An array of LEDs is mounted onto the rear flange to provide an optical background for certain tests.

Device	Image Region	7.4 MeV proton fluence (protons.cm^{-2})	7.4 MeV flux (protons.cm^{-2}.s^{-1})	10 MeV equivalent proton fluence (protons.cm^{-2})
Control	1	Control Device		
	2			
Room Temperature 1	1	3.03×10^{9}	2.0×10^{7}	4.0×10^{9}
	2	6.06×10^{9}	2.0×10^{7}	8.0×10^{9}
Room Temperature 2	1	1.21×10^{10}	2.0×10^{7}	1.6×10^{10}
	2	3.79×10^{10}	2.0×10^{7}	5.0×10^{10}
Cryogenic	1	6.06×10^{9}	2.0×10^{7}	8.0×10^{9}
	2	7.66×10^{10}	2.0×10^{7}	1.0×10^{11}

Table 2. Summary of devices to be proton irradiated and levels

During the cryogenic irradiation, the device will be irradiated with protons under nominal operating conditions. Immediate testing will then be performed whilst the device remains at cryogenic temperature and will consist of measurements of: conversion gain, noise, non-linearity, dark signal, dark signal non-uniformity, defects in darkness, charge injection uniformity, parallel & serial CTE and traps identified through trap-pumping. Once completed, the device will be allowed to warm to room temperature and allowed to anneal for periods of 1 day, 1 week and 1 month between repeated electro-optical testing to assess any annealing effects of the proton radiation damage.

8. CONCLUSIONS

This paper described a study currently underway for ESA to assess the quality and performance of seven devices procured from e2v technologies plc.

Initial results suggested that these devices offer n-channel like performance, but with significantly increased proton radiation hardness that could be useful in specific applications.

Further work and analysis is currently being undertaken and will be reported at a future date.

REFERENCES

[1] C. Bebek, *et al.*, "Proton Radiation Damage in P-channel CCDs Fabricated on High-Resistivity Silicon", IEEE Trans. Nucl. Sci., vol. 49 pp. 1221-1225, 2002

[2] Dawson, K., *et al.*, "Radiation Tolerance of Fully-Depleted P-Channel CCDs Designed for the SNAP Satellite", IEEE Trans. Nucl. Sci., vol. 55, no. 3 pp. 1725-1735, 2008

[3] Marshall, C., *et al.*, " Comparisons of the proton-induced dark current and charge transfer efficiency responses of n- and p-channel CCDs", Proc SPIE 5499, 2004

[4] Lumb, D., "CCD radiation damage in ESA Cosmic Visions missions: assessment and mitigation", Proc. SPIE 7439, 2009

[5] Hopkinson, G., "Proton damage effects on p-channel CCDs", IEEE Trans Nuc Sci, Vol 46, pages 1790-1796, 1999

[6] Jorden, P., *et al.*, "Commercialization of Full Depletion Scientific CCDs", Proc. SPIE 6276, 2006

[7] Murray, N.J., "Improvements to MOS CCD Technology for Future X-ray Astronomy Missions", Ph.D. Thesis, Brunel University, 2008

[8] Gow, Jason P. D., *et al.*, "Comparison of proton irradiated P-channel and N-channel CCDs", Nuclear Instruments and Methods in Physics Research Section A: Accelerators, Spectrometers, Detectors and Associated Equipment, 686 pp. 15–19, 2012

[9] CCD203-82 Back Illuminated Scientific CCD Sensor Datasheet, A1A-100014 CCD203 Issue2, January 2007

[10] Gow, J. P. D., *et al.*, "Proton damage comparison of an e2v technologies n-channel and p-channel CCD204", IEEE Transactions on Nuclear Science, 2014

[11] Murray, N. J., *et al.*, "Mitigating radiation-induced charge transfer inefficiency in full-frame CCD applications by 'pumping' traps", Proc. of SPIE, 845317, 2012

[12] Gow, J. P. D., *et al.*, "Assessment of space proton radiation-induced charge transfer inefficiency in the CCD204 for the Euclid space observatory", Journal of Instrumentation, 7(C01030), 2012

[13] Hall, D. J., *et al.*, "Determination of in situ trap properties in CCDs using a "single-trap pumping" technique", IEEE Transactions on Nuclear Science (In press)

[14] Mostek, N.J., *et al.*, "Charge trap identification for proton-irradiated p+ channel CCDs", Proc. of SPIE, 774216 2010

[15] Gow, J. P. D., *et al.*, "Development of a Cryogenic Irradiation Test Facility and the Initial Results from a CCD236 Swept Charge Device", PSD10, September 2014